*International Journal of Minerals, Metallurgy and Materials*
*Volume 19, Number 9, Sep 2012, Page 863*
**DOI: 10.1007/s12613-012-0640-0**

# SOFC composite electrolyte based on LSGM-8282 and zirconia or doped zirconia from zircon concentrate

*Fitria Rahmawati*[1,2], *Bambang Prijamboedi*[1], *Syoni Soepriyanto*[3], *and Ismunandar*[1]

1) Inorganic and Physical Chemistry Research Group, Faculty of Mathematics and Natural Sciences, Institut Teknologi Bandung, Jl. Ganesha 10 Bandung 40132, Indonesia
2) Research Group of Solid State & Catalysis, Chemistry Department, Sebelas Maret University, Jl. Ir. Sutami 36 A Kentingan Surakarta 57126, Indonesia
3) Metallurgical Engineering Research Group, Faculty of Mining and Petroleum Engineering, Institut Teknologi Bandung, Jl. Ganesha 10 Bandung 40132, Indonesia
(Received: 18 July 2011; revised: 10 October 2011; accepted: 6 November 2011)

**Abstract:** The aim of this research is to study zirconia-based electrolyte materials to increase the commercial value of zircon concentrate as a side product of tin mining industries. Synthesis of $CaO$-$Y_2O_3$-$ZrO_2$ (CYZ) and 8mol% $Y_2O_3$-$ZrO_2$ (8YSZ) was carried out by solid state reaction. The result shows that $ZrO_2$ presents in tetragonal phase. Doping of $Y_2O_3$ into $ZrO_2$ allows a phase transformation from tetragonal into cubic structure with small percentage of monoclinic phase. Meanwhile, doping of $CaO$-$Y_2O_3$ allows a phase transformation into a single cubic phase. These phase transformations enhance the ionic conductivity of the material. Introduction of 10wt% of LSGM-8282 into CYZ (CYZ-L90:10) allows further improvement of inter-grain contact shown by SEM morphological analysis and leads to the enhancement of ionic conductivity.

**Keywords:** solid oxide fuel cells (SOFC); solid electrolytes; LSGM electrolyte; zirconia; phase transformations; ionic conductivity

## 1. Introduction

The electrolyte material of yttria-stabilized zirconia (YSZ) has been extensively investigated during the last decade, and it is widely used in solid oxide fuel cells (SOFC) [1-3], which operate in the high temperature region of 850-1000°C. For the system of high temperature solid oxide fuel cells (HT-SOFCs), enormously high efficiencies can be achieved by its integration with a gas turbine for large-scale stationary applications [4]. Large HT-SOFC systems must be built in the stacking structure and they need various ceramics and high-temperature metal alloys, limiting the choice of materials. HT-SOFCs also face the problem of high corrosion rate of stacks. Therefore, for the reduction in cost and corrosion rate, there is always a demand to reduce the operating temperature of SOFC. Thus, any incremental improvement in the ionic conductivity of the electrolyte is meaningful for applications [5].

A considerable interest in the mixed dopant effect on the ionic conductivity in several ternary systems containing $ZrO_2$ and $Y_2O_3$ has arisen. These ternary systems have been studied from the viewpoint of structural and electrical properties. Oxides commonly used as the third component were calcia [6-8] or magnesia [9]. The mixed $CaO/Y_2O_3$-stabilized $ZrO_2$ (CYZ) exhibits comparable ionic conductivity to YSZ even at the operating temperature around 1000°C. This implies that the ternary system of $ZrO_2$-$Y_2O_3$-CaO may be more attractive than other ternary systems, mainly because of the lower cost of CaO compared to other trivalent oxides such as $Sc_2O_3$ [10] and $Yb_2O_3$ [11]. Bućko [12] has synthesized CYZ using the hydrothermal method from co-precipitated zirconia hydrogel and found that the fully cubic phase could be obtained after sintering at 1300°C. It has also been found that the substitution of calcia for yttria as well as yttria for calcia in the zirconia solid solutions led to an enhancement of ionic conductivity. In particular, for a sample with 8mol% oxygen vacancies (8C10Y90, the mass ratio of $CaO$:$Y_2O_3$ is 10:90), substitution of yttria for calcia caused a significant enhancement of bulk conductivity and grain boundary conductivity.

Corresponding author: Ismunandar, E-mail: ismu@chem.itb.ac.id; Fitria Rahmawati, E-mail: fitria@uns.ac.id

Ishihara *et al.* [13] found that $LaGaO_3$-based perovskite oxides, particularly with appropriate dopants such as Sr and Mg, have high oxide ion conductivity. These materials are considered as suitable electrolyte materials for SOFC for their high ionic conductivity at lower temperatures. In addition to the high ionic conductivity factor, thermo-mechanical properties, namely thermal expansion coefficient (TEC), morphological and geometrical stability in different atmospheres and mechanical toughness are among other important factors for the electrolyte material. All factors must also be considered for material selection and application at high temperature [14]. Based on (i) the similarity of TEC values between the lanthanum strontium gallate magnesite (LSGM) and zirconia-based electrolyte (the TEC of LSGM-8282 is $11.55\times10^{-6}$ $K^{-1}$ at 298-1273 K [15] and that of 8YSZ is $10.1\times10^{-6}$ $K^{-1}$ at 298-1273 K [16]), (ii) the superior stability of zirconia, and (iii) the high ionic conductivity of LSGM at lower temperatures, the combination of these two materials may afford a composite with high ionic conductivity at lower temperatures and good compatibility with the other components of the cell. Results of the synthesis and properties of the composites of zirconia with LSGM (ZL), CYZ with LSGM (CYZ-L), and 8YSZ with LSGM (YSZ-L) were reported in this paper.

## 2. Experimental

The zirconia ($ZrO_2$) material used in this research was prepared by caustic fusion of zircon ($ZrSiO_4$) and was obtained from $ZrSiO_4$ concentrate from a tin mining plant, Bangka Island, Indonesia. The other materials such as CaO (Aldrich, 99.995%), $Y_2O_3$ (Aldrich, 99.99%), $La_2O_3$ (Sigma Aldrich, 99.99%), MgO (Sigma Aldrich, 99.999%), $SrCO_3$ (Aldrich, 99.9%), $Ga_2O$ (Sigma Aldrich, 99.99%), and silver paste (SPI) were obtained from available commercial sources.

The synthesis of LSGM-8282 was carried out by solid state reaction. The required amounts of $La_2O_3$ and MgO were heated at 1000°C for 12 h before use. These materials were mixed with $SrCO_3$ and $Ga_2O$ and ground in acetone for 2 h followed by calcinations at 1100°C for 24 h with intermediate grinding. The LSGM-8282 disc finally was sintered at 1400°C for 36 h before impedance measurement.

Zirconia ($ZrO_2$) was prepared by caustic fusion of zircon concentrate ($ZrSiO_4$), *i.e.* by reacting zircon with NaOH, followed by acid leaching and precipitation of $ZrO_2$ through the addition of ammonia solution as described by Soepriyanto, *et al.* [17]. Doping of 8mol% $Y_2O_3$ into $ZrO_2$ was carried out by solid state reaction by introducing a certain amount of $Y_2O_3$ into zirconia powder to produce 8YSZ. Meanwhile, doping of CaO and $Y_2O_3$ to create 8mol% vacancies was also carried out by solid state reaction to produce CYZ ($Ca_{0.008}Y_{0.072}Zr_{0.862}O_{1.84}$). The mixed powder was ground and fired at 1350°C for 5 h for CYZ and at 1500°C for 5 h for 8YSZ.

Composites were prepared by introducing LSGM-8282 into $ZrO_2$, CYZ, and 8YSZ powders in the mass ratios of 90:10, 50:50, and 10:90, respectively. The mixed powder then was pressed into a disc and sintered at 1350°C for 5 h.

The synthesized materials were characterized by powder X-ray diffraction (XRD, PW 1710) using Cu $K_\alpha$ radiation. Refinements on XRD data were carried out using Le Bail methods implemented in Rietica program to determine their cell parameters. Morphological analysis was carried out by scanning electron microscopy (SEM, JEOL EO 1.1 JSM 6360). Ionic conductivity was measured by an LCR meter (Agilent E4980A) in the frequency of 20 Hz-2 MHz and at the temperature from 200 to 500°C. The data from impedance measurement were fitted using ZView program to determine the value of grain resistance ($R_g$), grain boundary resistance ($R_{gb}$), and electronic resistance.

## 3. Results and discussion

The XRD patterns and their refinement profiles for $ZrO_2$, YSZ, CYZ, and LSGM-8282 are shown in Figs. 1(a) and 1(b). The XRD pattern for $ZrO_2$ shows some broadened peaks. These broadened peaks indicate that $ZrO_2$ has small particle size. This is supported by SEM analysis, which shows that the average particle size of $ZrO_2$ is in the range of 48-80 nm. Meanwhile, XRD patterns of CYZ and YSZ show that doping of yttria and calcia-yttria enhances the crystallinity and enlarges the crystallite size of the materials, as appeared in the patterns of sharp peaks. It has been known that peak width is inversely proportional to crystallite size, as described in the Scherrer equation [18].

We could mention here that the XRD pattern for YSZ still shows the presence of monoclinic phase. This monoclinic phase almost disappears in the CYZ sample. The XRD pattern of LSGM-8282 synthesized by the solid state reaction method shows some sharp peaks indicating good crystallinity. However, the secondary phase of $LaSrGa_3O_7$ also exists as indicated by characteristic peaks at $2\theta$= 29.996°, 35.540°, and 49.586°.

XRD patterns of the composite of $ZrO_2$ with LSGM-8282

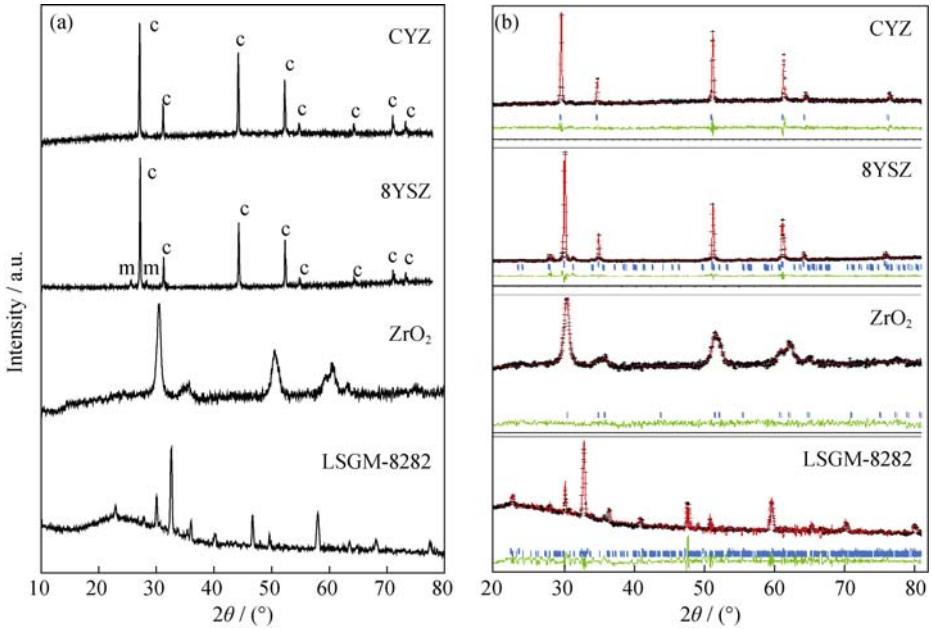


**Fig. 1. XRD patterns of LSGM-8282, $ZrO_2$, CYZ, and 8YSZ (c—cubic phase; m—monoclinic phase) (a) and the refinement profiles of the XRD patterns (b).**

in the mass ratio of 90:10 named as ZL90:10 and those in the mass ratio of 10:90 named as ZL10:90 are shown in Fig. 2. For the ZL90:10 sample, the XRD pattern shows the characteristics of an amorphous phase. Meanwhile, in the XRD pattern of ZL10:90 there are some characteristic peaks of LSGM, $ZrO_2$, and secondary phases, which are identified as as lanthanum zirconate ($La_2Zr_2O_7$) at $2\theta$=48.169° and $Ga_2O_3$ at $2\theta$=63.374°. These XRD results implied that the reaction between LSGM-8282 and $ZrO_2$ occurred in the composite.

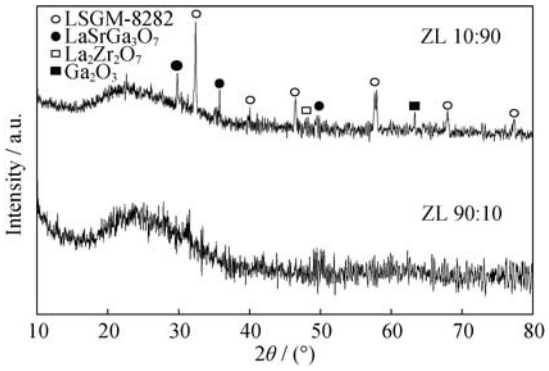


**Fig. 2. XRD patterns of $ZrO_2$-LSGM 90:10 (ZL90:10) and $ZrO_2$-LSGM 10:90 (ZL10:90).**

The addition of 10wt% of LSGM-8282 into CYZ allows the appearance of small peaks at $2\theta$=28.130°, which is identified as the monoclinic phase of zirconia and a peak of $La_4Sr_3O_9$ at $2\theta$=30.940°. XRD patterns of the composite of CYZ with LSGM, named as CYZ-L at various compositions are shown in Fig. 3. In the XRD pattern of CYZ-L50:50, the characteristic peaks of LSGM-8282 and $ZrO_2$ are presented. However, there are additional peaks of $LaSrGa_3O_7$ and $La_4Sr_3O_9$ at $2\theta$=27.925° and 63.580°, respectively. Meanwhile, in CYZ-L10:90 some characteristic peaks of cubic zirconia disappear and the XRD pattern is dominated by LSGM-8282 peaks. Another additional peak at $2\theta$=28.53° is identified as lanthanum zirconate, $La_2Zr_2O_7$. The XRD patterns indicate that the reaction between CYZ and LSGM-

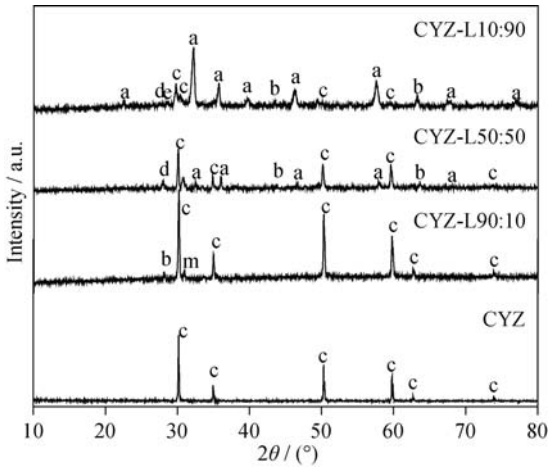


**Fig. 3. XRD patterns of CYZ and CYZ-L composites (a—characteristic peaks of LSGM-8282; b—$La_4Sr_3O_9$; c—cubic phases of zirconia; d—$LaSrGa_3O_7$; e—$La_2Zr_2O_7$; m—monoclinic phases of zirconia).**

8282 could occur in the composite. The secondary phase resulted from this reaction could be easily formed in the composite with large LSGM-8282 fraction.

The XRD pattern of the 10wt% of LSGM-8282 and 8YSZ composite shows that 8YSZ remains in cubic and monoclinic structure. However, the insulating phases of $LaSrGa_3O_7$ and $La_4Sr_3O_9$ appear after the addition of 50wt% of LSGM-8282 and 90wt% of LSGM-8282 into 8YSZ. The characteristic peak of $La_2Zr_2O_7$ is also seen in YSZ-L10:90 at $2\theta$=28.53°. The XRD patterns of the YSZ-L composite are given in Fig. 4.

Structural refinement of XRD data using the Le Bail method shows that the crystal structure of LSGM-8282 is cubic and the space group is *Pm*3*m*. The presence of secondary phases of $La_4Sr_3O_9$ and $LaSrGa_3O_7$ in LSGM has also been reported by others [19-20]. A Pechini-type chemical preparation route reported by Tąs *et al.* [19] also resulted in the secondary phase of $LaSrGa_3O_7$ and $LaSrGaO_4$. Furthermore, Majewski *et al.* [20] synthesized LSGM-8282 using the mixed route and found that after 24 h at 1400°C the powder consisted of a high content of LSGM and about 5vol% of $LaSrGa_3O_7$. The cell parameters of LSGM-8282 are listed in Table 1.

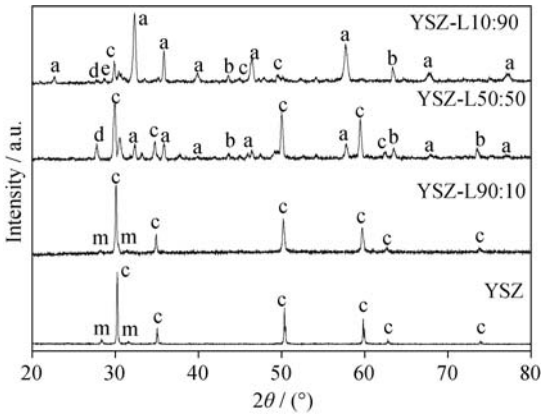


**Fig. 4. XRD patterns of YSZ and YSZ-L composites (a—characteristic peaks of LSGM-8282; b—$La_4Sr_3O_9$; c—cubic zirconia; d—$LaSrGa_3O_7$; e—$La_2Zr_2O_7$; m—monoclinic zirconia).**

**Table 1. Cell parameters of LSGM-8282, $ZrO_2$, CYZ, CYZ-L90:10, YSZ, and YSZ-L90:10**

| Parameter | $La_{0.8}Sr_{0.2}Ga_{0.8}Mg_{0.2}O_{3-\delta}$ | | $ZrO_2$ | CYZ | CYZ-L90:10 | | YSZ | | YSZ-L90:10 | |
|---|---|---|---|---|---|---|---|---|---|---|
| | Cubic (*Pm*3*m*) | $LaSrGa_3O_7$ | Tetragonal (*P*42/*nmc*) | Cubic (*Fm*3*m*) | Cubic (*Fm*3*m*) | Monoclinic (*P*21) | Cubic (*Fm*3*m*) | Monoclinic (*P*21) | Cubic (*Fm*3*m*) | Monoclinic (*P*21) |
| *a* / nm | 0.39018(7) | 0.8049(2) | 0.360(1) | 0.5150(3) | 0.51319(2) | 0.5301(2) | 0.51313(3) | 0.5354(1) | 0.51407(7) | 0.5357(1) |
| *b* / nm | 0.39018(7) | 0.8049(2) | 0.360(1) | 0.5150(3) | 0.51319(2) | 0.5268(2) | 0.51313(3) | 0.5295(1) | 0.51407(7) | 0.5290(1) |
| *c* / nm | 0.39018(7) | 0.5336(2) | 0.522(2) | 0.5150(3) | 0.51319(2) | 0.5139(2) | 0.51313(3) | 0.5092(8) | 0.51407(7) | 0.5092(1) |
| $R_p$ / % | 5.305 | — | 2.645 | 4.828 | 4.41 | — | 7.870 | — | 4.16 | — |
| $R_{wp}$ / % | 4.989 | — | 3.011 | 6.210 | 6.26 | — | 5.410 | — | 5.24 | — |
| $\chi^2$ | 0.24 | — | 0.063 | 0.483 | 0.463 | — | 0.176 | — | 0.255 | — |

Structural refinement on the XRD data of $ZrO_2$ shows that $ZrO_2$ is in tetragonal structure. Meanwhile, doping of calcia-yttria into $ZrO_2$ allows the transformation to fully cubic structure. However, doping of 8mol% of yttria into $ZrO_2$ transforms tetragonal zirconia to cubic and monoclinic phases. The cell parameters of $ZrO_2$, CYZ, and 8YSZ are listed in Table 1. The cubic lattice parameter of CYZ is 0.5150(3) nm. The cell parameter of CYZ is higher than that of 8YSZ which is 0.51313(3) nm. The complete description about 8YSZ and CYZ, which have been prepared from zircon ($ZrSiO_4$) concentrate, has been published previously [21].

Le Bail refinement on CYZ-L90:10 proceeds successfully in two phases of cubic *Fm*3*m* and monoclinic *P*21. The existence of monoclinic phase and secondary phase of $La_4Sr_3O_9$ indicates that a reaction possibly occurred in this composite during the sintering process. This is supported by the change of cell parameter from 0.5150(3) nm for CYZ to 0.51319(2) nm for the cubic phase in CYZ-L90:10. Meanwhile, the refinement on 8YSZ and YSZ-L90:10 proceeds successfully in cubic structure *Fm*3*m* and monoclinic *P*21. The cell parameter of YSZ-L90:10 is 0.51407(7) nm which is higher than that of YSZ, *i.e.* 0.51313(3) nm. This may also indicate that a chemical reaction occurred during the sintering process. This chemical reaction may produce defects in crystal structure. Interstitial defects, known as Frenkel defects, do perturb the host structure in the immediate vicinity of the interstitial atom. Meanwhile the presence of vacancies due to the doping process in ionic crystals appears to cause a relaxation of the structure in the immediate environment of the vacancy and produce the relaxation of atoms outwards because of an imbalance in electrostatic forces

[22]. Cell parameters of the phases existing in CYZ-L90:10 and YSZ-L90:10 are also listed in Table 1.

Ionic conductivity measurement on $ZrO_2$, 8YSZ, and CYZ gave the conductivity values in the temperature range from 200 to 500°C, shown in Fig. 5. The conductivity values of $ZrO_2$ are below $10^{-4}$ S·cm$^{-1}$, which is far below the range of conductivity of good electrolytes [23]. Doping of zirconia with yttria and calcia-yttria greatly improves their ionic conductivity because of the phase transformation from tetragonal into cubic as shown in the XRD data. In general, the ionic conductivity of 8YSZ is higher than that of CYZ as described in the Arrhenius plot (Fig. 5). The 8YSZ sample also has a lower activation energy, indicating that the movement of ions from the crystal lattice and the migration of ions occur easier in 8YSZ than in CYZ. However, the higher value of the pre-exponential factor of CYZ, 6.927, compared with that of 8YSZ, 4.257, as listed in Table 2, indicates that CYZ could have a higher ionic conductivity at high temperature. The pre-exponential factor extracted from the Arrhenius equation is a function of the charge carrier concentration [24]. The Arrhenius equation is described as

$$\sigma T = \sigma_o \exp\left(\frac{-E_a}{kT}\right) \tag{1}$$

where $E_a$ is the activation energy for ionic conduction, $\sigma$ the ionic conductivity, $\sigma_o$ the pre-exponential factor, $k$ the Boltzmann constant, and $T$ the temperature. The pre-exponential factor is a function of defect concentration. Eq. (2) defines the pre-exponential factor for Frenkel defects, and Eq. (3) defines the pre-exponential factor for Schottky defects [22]:

$$\sigma_0 \equiv \frac{n_f}{\exp(-g_f/2kT)}(a^2q^2/kT)\upsilon_o \tag{2}$$

$$\sigma_o \equiv \frac{n_s}{\exp(-g_s/2kT)}(a^2q^2/kT)\upsilon_o \tag{3}$$

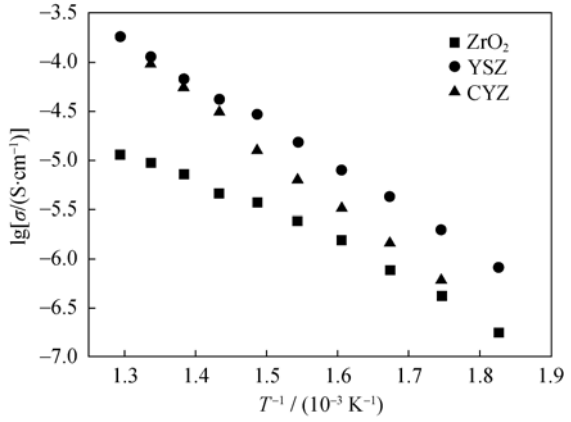


**Fig. 5. Arrhenius plots of CYZ, 8YSZ, and $ZrO_2$.**

**Table 2. Comparison of activation energy ($E_a$) and pre-exponential factor of CYZ, CYZ-L90:10, YSZ, and YSZ-L90:10**

| Samples | Activation energy, $E_a$ / eV | Pre-exponential factor, $\ln\sigma_o$ |
|---|---|---|
| CYZ | 1.047 | 6.927 |
| CYZ-L90:10 | 1.171 | 9.213 |
| CYZ-L50:50 | 1.119 | 7.725 |
| CYZ-L10:90 | 0.953 | 3.254 |
| YSZ | 0.859 | 4.257 |
| YSZ-L90:10 | 1.012 | 5.604 |
| YSZ-L50:50 | 1.178 | 5.674 |
| YSZ-L10:90 | 1.036 | 2.441 |

where $n_f$ is the pre-exponential factor for Frenkel defects and $n_s$ for Schottky defects, $a$ is the interatomic space, $q$ the charge, $v_o$ the vibrational frequency, $T$ the absolute temperature, and $g_f$ and $g_s$ are the defect formation energies for Frenkel defects and Schottky defects, respectively.

The charge carrier in oxygen ion conductors is the oxygen vacancy; therefore, the pre-exponential factor is a function of defect concentration. At low temperature, oxygen vacancies are associated with the cations which were doped into the host crystal and forming cluster. For example, in YSZ oxygen vacancies exist in two modes: $Y'_{Zr}V_O^{\bullet\bullet}$ and $V_O^{\bullet\bullet}$. The binding of some oxygen vacancies to yttrium ions made the oxygen vacancies unavailable for conduction. Therefore, it requires a supplemental energy to free oxygen vacancies from $Y'_{Zr}V_O^{\bullet\bullet}$ [24], so the activation energy at low temperature is the sum of dissociation and migration energy of these oxygen vacancies. Meanwhile, at high temperature oxygen vacancies are assumed to be in free condition; therefore, the activation energy only represents the migration energy of these oxygen vacancies [24]. The linear equations of CYZ and 8YSZ intersect at 547°C. This means that above 547°C the ionic conductivity of CYZ becomes higher than that of YSZ as can be seen in Fig. 5.

To study the effect of LSGM-8282 introduction into CYZ and 8YSZ, the total ionic conductivity values of the composites are plotted against temperature and the results are given in Fig. 6. The conductivity values of CYZ and CYZ-L90:10, in general, are similar. However, it can be seen that in the higher temperature region, the conductivity of CYZ-L90:10 is higher than that of CYZ. Therefore, we could expect that CYZ-L90:10 has potential application as an electrolyte material in intermediate temperature SOFC (IT-SOFC), which is operated at 600-800°C. However, the introduction of 50wt% and 90wt% of LSGM tends to reduce the ionic conductivity of CYZ.

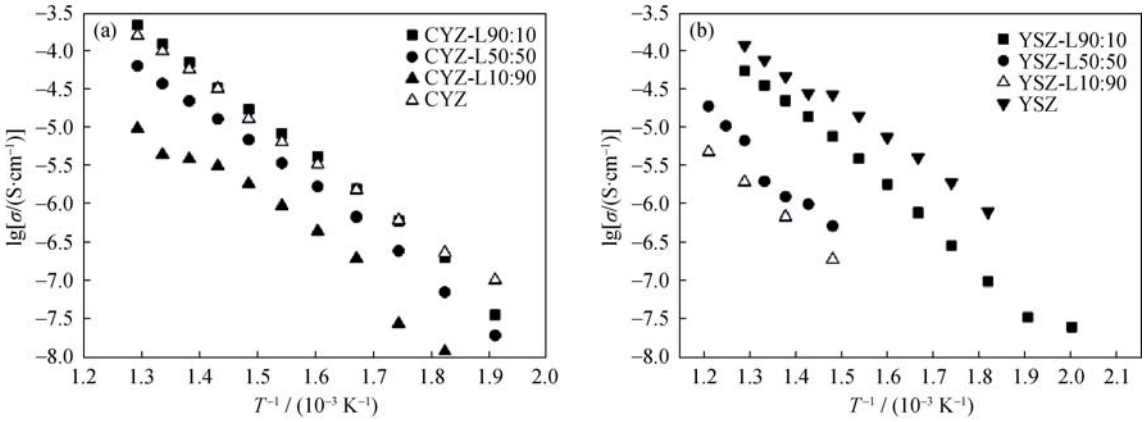


**Fig. 6. Arrhenius plots of the total ionic conductivity of CYZ-L (a) and YSZ-L (b).**

It is interesting to study the factors that contribute to the increase of ionic conductivity in the CYZ-L90:10 composite. It should look into the impedance data of CYZ and CYZ-L at 350°C, shown in Fig. 7. For the CYZ and CYZ-L90:10 samples, the impedance data give two clear semicircles indicating the grain and intergrain conductivities. The presence of LSGM- 8282 mainly reduces the intergrain conductivity. For the samples with higher LSGM-8282 content, it tends to show one large semicircle. This might give an indication that a different conductivity mechanism occurs, probably due to the reaction between those phases. The Arrhenius plots of the conductivity data for CYZ and CYZ-L90:10 are given in Fig. 8. In the CYZ sample, both grain and grain boundary conductivities have the similar slope. The CYZ-L90:10 has the grain and grain boundary conductivities with different slopes. At high temperature, the grain boundary conductivity is higher than the grain conductivity. This indicates the significant contribution of grain boundary conductivity to the total ionic conductivity because of the decrease of resistance between grains as the grains are better connected each other after introducing 10wt% of LSGM into CYZ.

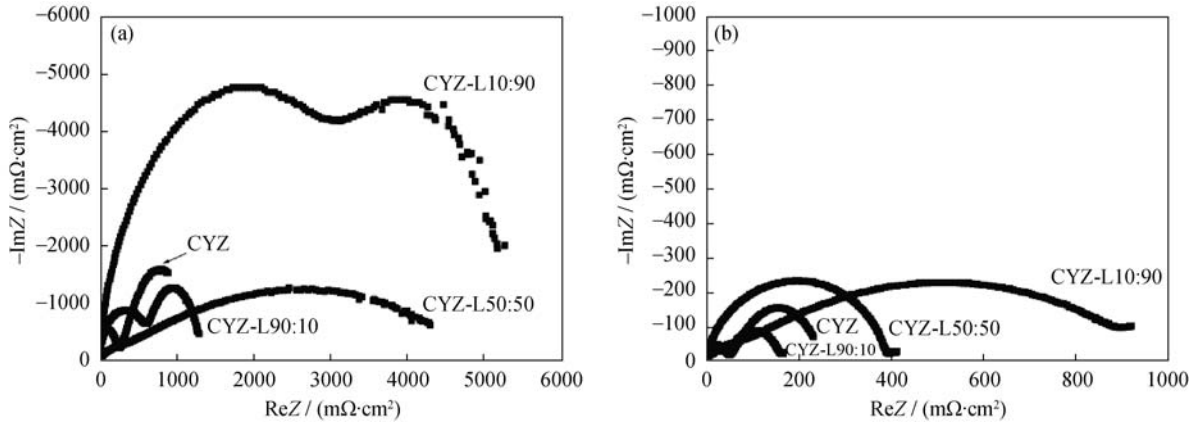


**Fig. 7. Typical impedance spectra of CYZ and CYZ-L at 300 (a) and 350°C (b).**

The SEM image of CYZ (Fig. 9(a)) shows rough morphology, small grains and blocking phases, which are highly distributed and those small grains were identified by EDX analysis as silica-rich phases, and the EDX profile is depicted in Fig. 10. The blocking phases in CYZ present as grains that have small size compared to the blocking phases in CYZ-L90:10 which are shown by the white arrow in Fig. 9(b). Meanwhile, the SEM image of CYZ-L90:10 shows better contact between grains as described in Fig. 9(c) and larger grains of blocking phase, which is identified by EDX analysis as silica-rich phase (Fig. 10). EDX analysis shows that the blocking phase in CYZ-L90:10 has a silica content of 8.76wt%. This is higher than the silica content in blocking phases of CYZ, 6.36wt%. This indicates that the addition of 10wt% of LSGM-8282 into CYZ forces silica out of the bulk phase and aggregates into larger grains and distributes only in some definite places. The SEM images of CYZ-L50:50 and CYZ-L10:90 show more roughness morphology than CYZ-L90:10. Apparently, small addition of LSGM-8282 into CYZ enhances the interconnection among

grains; however, the presence of CYZ in the phase dominated by LSGM-8282 tends to inhibit the sintering process. The good interconnection between grains is a factor that results in CYZ-L90:10 and has a higher conductivity than other compositions of CYZ-L. In addition, the existence of insulating phases of $LaSrGa_3O_7$, $La_3Sr_4O_9$, and $La_2Zr_2O_7$ will also result in the low ionic conductivity of CYZ-L50:50 and CYZ-L10:90.

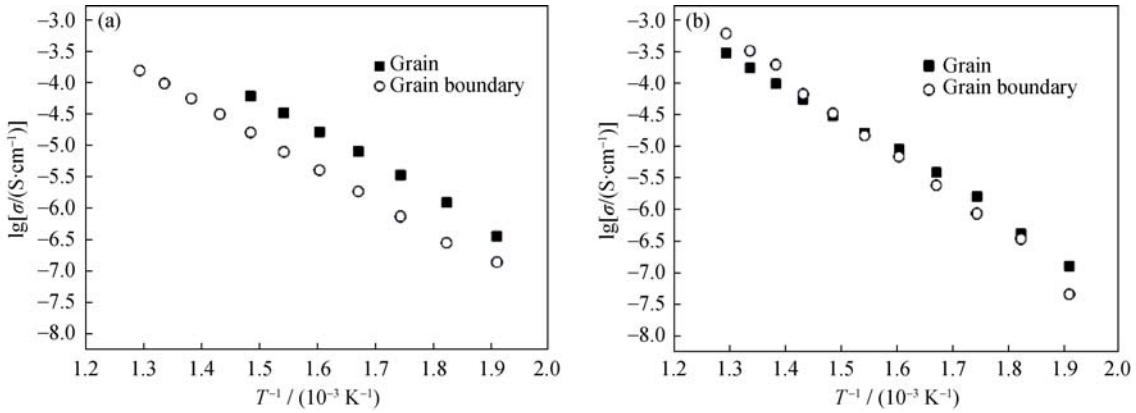


**Fig. 8. Comparison of grain and grain boundary conductivities of CYZ (a) and CYZ-L90:10 (b).**

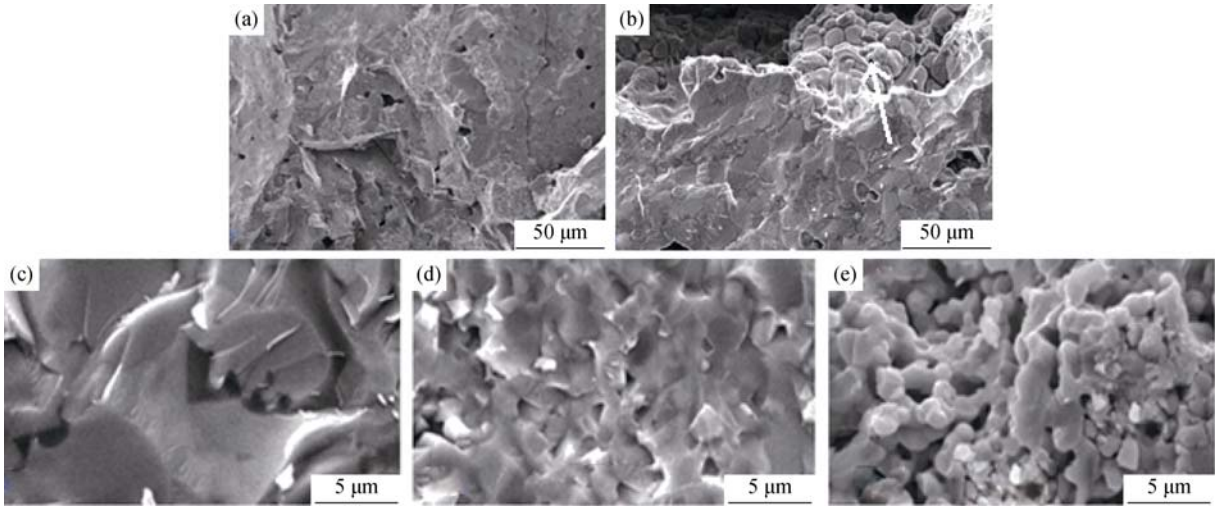


**Fig. 9. SEM images of CYZ (a), CYZ-L90:10 (b, c), CYZ-L50:50 (d), and CYZ-L10:90 (e).**

The calculation of activation energy shows that the activation energy of CYZ is 1.047 eV and becomes 1.171 eV after the addition of 10wt% of LSGM-8282. It means that a higher energy is required to create oxygen vacancies and to migrate the oxygen ions in CYZ-L90:10. This leads to the reduction in ionic conductivity of CYZ-L90:10, so it becomes lower than that of CYZ at low temperature (<325°C). However, at higher temperature (>325°C) the increase in ionic conductivity of CYZ-L90:10 is larger than that of CYZ. This enhancement is possibly due to the higher oxygen vacancy concentration in CYZ-L90:10 as shown by the higher pre-exponential factor value of CYZ-L90:10 than that of CYZ. On the contrary, the addition of 50wt% and 90wt% of LSGM-8282 tends to reduce the pre-exponential value.

The addition of 10wt% LSGM-8282 increases the activation energy from 0.859 eV for YSZ to 1.012 eV for YSZ-L90:10. However, based on the trend of the Arrhenius plots given in Fig. 6, there is a possibility that YSZ-L90:10 has high ionic conductivity above 500°C. This is supported by the pre-exponential factor of YSZ-L90:10, 5.604, which is higher than that of YSZ, 4.257. This indicates that YSZ-L90:10 has a higher oxygen vacancy concentration than YSZ, so at high temperature when the oxygen vacancies are free, YSZ-L90:10 could have a higher ionic conductivity. YSZ-L50:50 also has the pre-exponential factor higher than that of YSZ. However, the existence of insulating phases of $LaSrGa_3O_7$ and $LaSr_3O_9$ seems to inhibit the

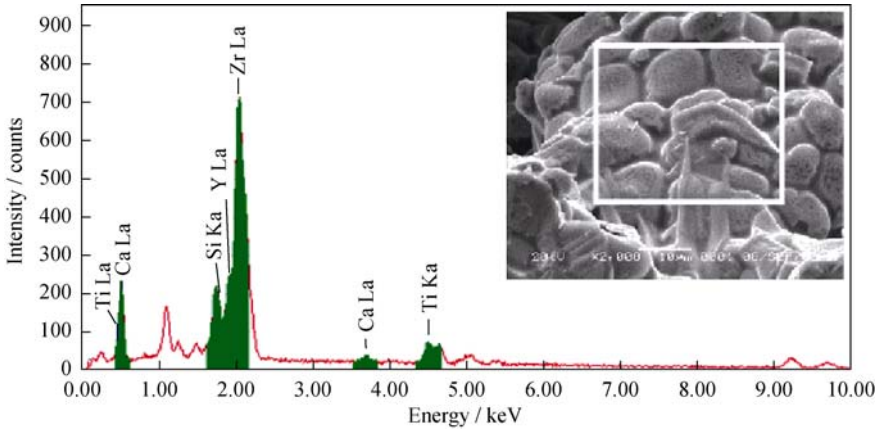


| Element | Transition energy / keV | Content / wt% | Error / % | Content / at% | Compound | Content / at% | Content / wt% | Cation / % |
|---|---|---|---|---|---|---|---|---|
| O | — | 28.10 | — | — | — | — | — | — |
| Si K | 1.739 | 4.09 | 0.40 | 16.99 | $SiO_2$ | 8.76 | 1.99 | 5.8881 |
| Ca K | 3.690 | 1.17 | 0.62 | 3.41 | CaO | 1.64 | 0.40 | 1.7590 |
| Ti K | 4.508 | 1.87 | 0.83 | 4.56 | $TiO_2$ | 3.12 | 0.53 | 2.5861 |
| Y L | 1.922 | 12.42 | 1.47 | 8.14 | $Y_2O_3$ | 15.77 | 1.91 | 16.7416 |
| Zr L | 2.042 | 52.34 | 0.98 | 66.90 | $ZrO_2$ | 70.71 | 7.84 | 73.0251 |
| Total | — | 100.00 | — | 100.00 | — | 100.00 | 12.68 | — |

**Fig. 10. EDX analysis on the blocking phase of CYZ-L90:10 (La means the electron transition from M to L shell, Ka means the electron transition from L to K shell, and the composition of each element in the form of its positive ion (cation) is listed in the last column.**

migration of oxygen ions, so it needs a higher activation energy to force ionic conduction, *i.e.* 1.178 eV.

Generally, the ionic conductivity of LSGM-8282 is still higher than that of other prepared materials as summarized in Fig. 11. Meanwhile, CYZ-L90:10 has a lower ionic conductivity than YSZ at low temperature; however, it becomes comparable to YSZ at 425°C. This is a promising result since other researchers [7-8] found that zirconia-stabilized $CaO/Y_2O_3$ shows a comparable conductivity value around

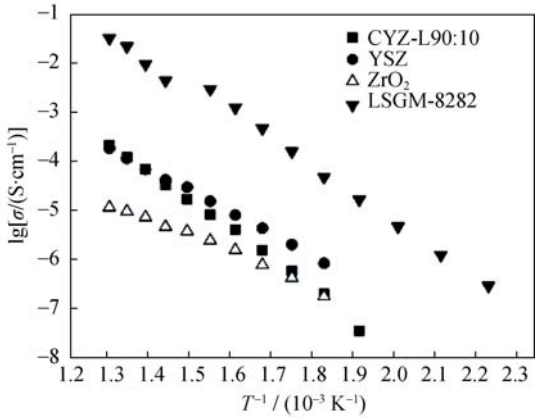


**Fig. 11. Comparison of the Arrhenius plots of LSGM-8282, $ZrO_2$, 8YSZ, and CYZ-L90:10.**

1000°C. Although CYZ-L90:10 has a lower ionic conductivity than LSGM-8282, this composite has better mechanical properties than LSGM-8282 as shown in the results of hardness measurement (Table 3). The greater the hardness of the material, the greater the resistance to deformation, scratches, and abrasion [25].

**Table 3. Hardness measurement results of LSGM-8282, $ZrO_2$, CYZ, CYZ-L90:10, YSZ, and YSZ-L90:10**

| Samples | Average Vickers hardness |
|---|---|
| LSGM-8282 | 86.57 |
| $ZrO_2$ | 120.97 |
| CYZ | 276.13 |
| CYZ-L90:10 | 261.03 |
| YSZ | 341.20 |
| YSZ-L90:10 | 310.90 |

Note: Hardness was measured at 3 points for each material and the average values are listed.

## 4. Conclusion

Zirconia synthesized from zircon concentrate present in tetragonal phase. Doping of 8mol% of $Y_2O_3$ allows phase

transformation into cubic and monoclinic phases, and doping of $CaO$-$Y_2O_3$ allows phase transformation from tetragonal into cubic single phase. The doped zirconia has a higher ionic conductivity than the undoped zirconia. Introduction of 10wt% of LSGM-8282 into CYZ allows the improvement of inter-grain contact and increases the oxygen vacancy concentration. This improvement reduces the grain boundary resistance and increases the ionic conductivity of CYZ-L90:10.

## Acknowledgements

This work was supported by the Directorate General of Higher Education, Republic of Indonesia through Hibah Desertasi Doktor and Riset KK ITB. Authors greatly acknowledge for this support. We also acknowledge to Prof. Gyeong Man Choi and the members of the Fuel Cell Laboratory, Pohang University of Science and Technology (POSTECH) for all the assistance provided.

## References

[1] X. Guo, Property degradation of tetragonal zirconia induced by low-temperature defect reaction with water molecules, *Chem. Mater.*, 16(2004), p.3988.

[2] T. Mori, J. Drennan, J.H. Lee, J.G. Li, and T. Ikegami, Oxide ionic conductivity and microstructures of Sm- or La-doped $CeO_2$-based systems, *Solid State Ionics,* 154-155(2002), p.461.

[3] A. Rizea, D. Chirlesan, C. Petot, and G. Petot-Ervas, The influence of alumina on the microstructure and grain boundary conductivity of yttria-doped zirconia, *Solid State Ionics*, 146(2002), No.3, p.341.

[4] D.J.L. Brett, A. Atkinson, N.P. Brandon, and S.J. Skinner, Intermediate temperature solid oxide fuel cells, *Chem. Soc. Rev.*, 37(2008), p.1568.

[5] A. Rizea, G. Petot-Ervas, C. Petot, M. Abrudeanu, M.J. Graham, and G.I. Sproule, Transport properties of yttrium-doped zirconia influence of kinetic demixing, *Solid State Ionics*, 177(2007), No.39-40, p.3417.

[6] J.H. Gong, Y. Li, Z.T. Zhang, and Z.L. Tang, ac impedance study of zirconia doped with yttria and calcia, *J. Am. Ceram. Soc.*, 83(2000), p.648.

[7] J.H. Gong, Y. Li, Z.L. Tang, and Z.T. Zhang, Ionic conductivity in the ternary system $(ZrO_2)_{1-0.08x-0.12y}$-$(Y_2O_3)_{0.08x}$-$(CaO)_{0.12y}$, *J. Mater. Sci.*, 35(2000), p.3547.

[8] Y. Li, M. Liu, J.H. Gong, Y. Chen, Z.L. Tang, and Z.T. Zhang, Grain-boundary effect in zirconia stabilized with yttria and calcia by electrical measurements, *Mater. Sci. Eng. B*, 103(2003), p.108.

[9] R. Chaim, Microstructure and bending strength in the ternary (Mg-Ca)-partially-stabilized zirconia, *J. Am. Ceram. Soc*., 75(1992), p.694.

[10] H. Kaneko, F.X. Jin, and H. Taimatsu, Electrical conductivity of zirconia stabilized with scandia and yttria, *J. Am. Ceram. Soc.*, 76(1993), No.3, p.793.

[11] R. Chiba, T. Ishii, and F. Yoshimura, Temperature dependence of ionic conductivity in $(1–x)ZrO_2$-$(x–y)Sc_2O_3$-$yYb_2O_3$ electrolyte material, *Solid State Ionics*, 91(1996), p.249.

[12] M.M. Bućko, Ionic conductivity of $CaO$-$Y_2O_3$-$ZrO_2$ materials with constant oxygen vacancy concentration, *J. Eur. Ceram. Soc.*, 24(2004), p.1305.

[13] T. Ishihara, J.A. Kilner, M. Honda, and Y. Takita, Oxygen surface exchange and diffusion in the new perovskite oxide ion conductor $LaGaO_3$, *J. Am. Chem. Soc.*, 119(1997), p.2747.

[14] F. Tietz, Thermal expansion of SOFC materials, *Ionics*, 5(1999), p.129.

[15] T. Ishihara, M. Honda, T. Shibayana, H. Minami, H. Nishiguchi, and Y. Takita, Intermediate temperature solid oxide fuel cells using a new $LaGaO_3$ based oxide ion conductor, *J. Electrochem. Soc.*, 145(1998), p.3177.

[16] H. Hayashi, T. Saitou, N. Maruyama, H. Inada, K. Kawamura, and M. Mori, Thermal expansion coefficient of yttria stabilized zirconia for various yttria contents, *Solid State Ionics*, 176(2005), p.613.

[17] S. Soepriyanto, A.A. Korda, and T. Hidayat, Development of zircon base industrial product from zircon-sand concentrate of Bangka tin processing, [in] *Proceeding of the 3rd International Workshop on Earth Science and Technology*, Fukuoka, 2005.

[18] J.I. Langford and A.J.C. Wilson, Scherrer after sixty years: a survey and some new results in the determination of crystallite size, *J. Appl. Crystallogr.,* 11(1978), p.102.

[19] A.C. Taş, P.J. Majewski, and F. Aldinger, Chemical preparation of pure and strontium and/or magnesium-doped lanthanum gallate powders, *J. Am. Ceram. Soc.*, 83(2000), p.2954.

[20] P. Majewski, M. Rozumek, C.A. Taş, and F. Aldinger, Processing of $(La,Sr)(Ga,Mg)O_3$ solid electrolyte, *J. Electroceram.*, 8(2002), p.65.

[21] F. Rahmawati, B. Prijamboedi, S. Soepriyanto, and Ismunandar, Doping calcia and yttria into zirconia obtained from by product of tin concentrator to improve its ionic conductivity, *ITB J. Sci.*, 43A(1) (2011), No.1, p.9.

[22] A.R. West, *Basic Solid State Chemistry,* 2nd Ed., John Wiley & Sons, Ltd., New York, 1999.

[23] R.C. Agrawal and R.K. Gupta, Review superionic solids: composite electrolyte phase—an overview, *J. Mater. Sci.*, 34(1999), p.1131.

[24] J.H. Gong, Y. Li, Z.L. Tang, Y.S. Xie, and Z.T. Zhang, Temperature-dependence of the lattice conductivity of mixed calcia/yttria-stabilized zirconia, *Mater. Chem. Phys.*, 76(2002), p.212.

[25] E. Oberg, F. Jones, H. Ryffel, C. McCauley, and R. Heald, *Machinery's Handbook 28th Edition*, Industrial Press, New York, 2008.